

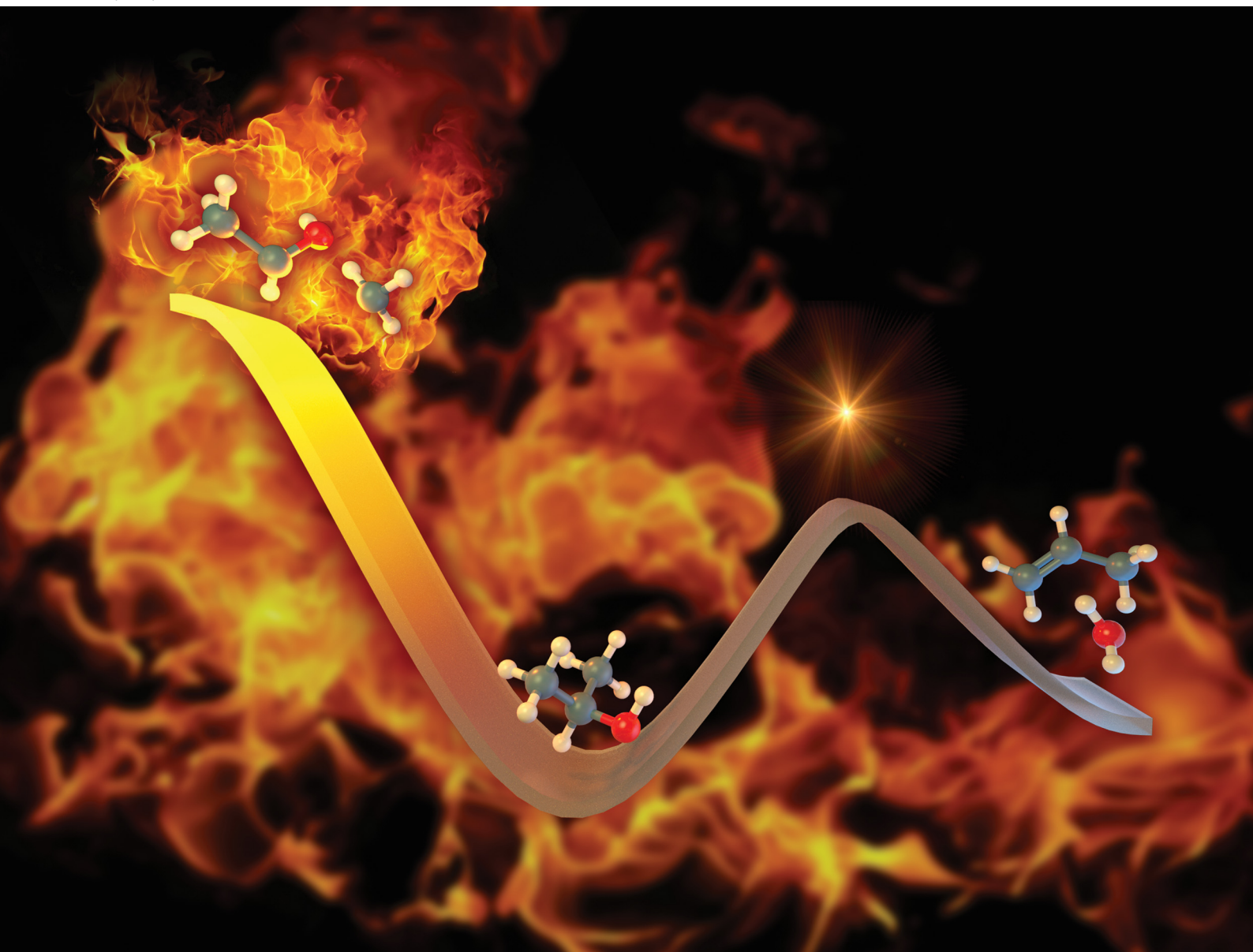
Volume 27  
Number 39  
21 October 2025  
Pages 20955–21346

# PCCP

Physical Chemistry Chemical Physics

rsc.li/pccp

**25**  
YEARS  
ANNIVERSARY



ISSN 1463-9076

 ROYAL SOCIETY  
OF CHEMISTRY

**PAPER**

Robert S. Tranter *et al.*  
Direct measurements for the kinetics of C–C bond fission in  
the high temperature decomposition of isopropanol

 **PCCP**  
Owner Societies


 Cite this: *Phys. Chem. Chem. Phys.*, 2025, 27, 20983

# Direct measurements for the kinetics of C–C bond fission in the high temperature decomposition of isopropanol

 John H. Kim,<sup>id</sup><sup>ab</sup> Keunsoo Kim,<sup>†b</sup> Sebastian L. Peukert,<sup>‡b</sup> Joe V. Michael,<sup>§b</sup> Raghu Sivaramakrishnan,<sup>id</sup><sup>b</sup> Margaret S. Wooldridge<sup>ac</sup> and Robert S. Tranter<sup>id</sup><sup>\*b</sup>

The thermal decomposition of isopropanol was studied experimentally and theoretically with a view to isolate and directly measure rate coefficients for the dominant radical channel in this multi-channel process. Two complementary shock tube methods, laser schlieren densitometry and H-atom atomic resonance absorption spectroscopy, were used to obtain rate coefficients for the C–C bond fission channel. The experimental ranges span temperatures from 1200–2100 K and pressures between 30–690 torr. These are the most direct measurements of this rate coefficient in the fall-off regime of relevance to high-temperature reacting systems. Theoretical studies also performed in this work confirm that the title reaction and a molecular elimination involving dehydration were the sole unimolecular processes at high temperatures. A master equation analysis yielded  $k(T, P)$  for the C–C fission and these are shown to be in good agreement with the present experimental measurements. Comparisons with prior experimental and theoretical studies in the literature indicate branching ratios as well as absolute  $k(T, P)$  for C–C bond-fission have been under-predicted for this decomposition reaction. Consequently, results from the present studies place an increased emphasis on radical-driven secondary processes in high-temperature pyrolysis of this simplest secondary alcohol.

 Received 30th June 2025,  
 Accepted 19th August 2025

DOI: 10.1039/d5cp02482j

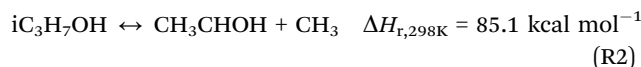
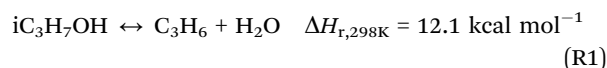
[rsc.li/pccp](http://rsc.li/pccp)

## Introduction

The high-temperature chemistry of alcohols is of fundamental importance in combustion and fuel utilization. In contrast with ethanol and butanol, the pyrolysis chemistry of propanol, in particular isopropanol, has significant deficiencies that limit the ability to develop predictive kinetic models for combustion systems and other applications. Recent studies have provided new data for understanding elementary reaction pathways in isopropanol pyrolysis. However, critical differences between model predictions and experimental data remain. For example, Burnett *et al.*<sup>1</sup> found significant discrepancies between model predictions and experimental measurements of isopropanol pyrolysis at high temperature ( $T > 900$  K) and high pressure

(5 bar), indicating the initial thermal decomposition rate coefficients may be incorrect.

In the recent shock-tube study of isopropanol decomposition by Kim *et al.*,<sup>2</sup> time-of-flight mass spectrometry was used to measure major products and intermediate species for temperatures of 1395–2053 K and pressures of 0.3–4 bar. At these conditions, dissociation of isopropanol was identified to occur by two channels: (R1) a dehydration yielding propene, and (R2) a methyl radical elimination with a co-product 1-hydroxyethyl radical.



Dissociation of isopropanol by reactions (R1) and (R2) agrees with other studies. However, quantifications of the rate coefficients,  $k_1$  and  $k_2$ , are limited as are the temperature and pressure dependencies of the branching ratios to these two channels. In the computational study by Bui *et al.*,<sup>3</sup>  $k_1$  and  $k_2$  were calculated using variational RRKM theory to determine the low- and high-pressure limits, as well as the values at 50 torr and 760 torr. Bui *et al.* concluded that at lower pressures

<sup>a</sup> Department of Mechanical Engineering, University of Michigan, Ann Arbor, MI, US

<sup>b</sup> Chemical Sciences and Engineering Division, Argonne National Laboratory, Lemont, IL, US

<sup>c</sup> Department of Aerospace Engineering, University of Michigan, Ann Arbor, MI, US

<sup>†</sup> Current address: Center for Hydrogen and Fuel Cell Research, Korea Institute of Science and Technology (KIST), Seoul 02792, Republic of Korea.

<sup>‡</sup> Current address: Deutsche Forschungsgemeinschaft e.V. (DFG), Bonn, Germany.

<sup>§</sup> Deceased.


(below 760 torr) the water elimination reaction, (R1), was the primary reaction channel. At higher pressures and at  $T > 1200$  K, the bond-scission reaction, (R2), was predicted to be the dominant reaction channel. While the predicted values for  $k_2$  were in agreement with the estimates from Tsang,<sup>4</sup> the  $k_1$  values from theory were shown to underpredict the experimentally determined  $k_1$  values (obtained by monitoring  $C_3H_6$  formation) from Trenwith.<sup>5</sup> Apart from the extensive theoretical kinetics study by Bui *et al.*, there is a theoretical study from Pokidova *et al.*<sup>6</sup> that considered only the dehydration channel, (R1), from isopropanol. A more recent study from Buerger *et al.*<sup>7</sup> also calculated theoretical kinetics for (R1) and (R2) as a simpler analogy for the decomposition kinetics of titanium tetraisopropoxide.

Since the theoretical studies by Bui *et al.*<sup>3</sup> there have been a few high-temperature experimental studies of isopropanol pyrolysis and decomposition, mainly focusing on (R1). Heyne *et al.*<sup>8</sup> used a variable-pressure flow reactor to determine the kinetics for isopropanol decomposition at 12.5 atm and 976–999 K. From simulations of their experimental results, Heyne *et al.* obtained  $k_1$  values that were higher than the Bui *et al.*<sup>3</sup>  $k_{1,\infty}$  values by about a factor of 4. Rosado-Reyes *et al.*<sup>9</sup> characterized the kinetics for the dehydration channel in isobutanol and using this information and data from prior studies in their laboratory on other alcohols, they were able to derive a rate expression for reaction (R1) over the  $T$ -range from 1000–1250 K and 1.5–6 atm. In contrast with Heyne *et al.*, the  $k_1$  values from Rosado-Reyes *et al.*<sup>9</sup> are within a factor of 1.5 of the Bui *et al.*<sup>3</sup> predictions. Jouzdani *et al.*<sup>10</sup> performed shock tube pyrolysis studies over 1300–1550 K and 3.5–11 atm. They used laser absorption to monitor CO formation and simulated the profiles with a variety of models from the literature. Li *et al.*<sup>11</sup> studied the pyrolysis of isopropanol in a flow tube (900–1350 K, 0.04–1 atm) with photoionization mass spectrometry. Due to the discrepancies between theoretical calculations for isopropanol decomposition reactions and the available experimental data, Li *et al.* simulated their experimental results with a reaction mechanism based on analogies with butanol pyrolysis. Notably, there are significant differences in the rate coefficients and branching ratios for (R1) and (R2) between the recommendations by Bui *et al.*<sup>3</sup> and the analogy-based kinetics from Li *et al.*<sup>11</sup> Lastly, there have been two recent shock tube studies that also characterized the dehydration channel in isopropanol decomposition. Mertens and Manion<sup>12</sup> used a single-pulse shock tube to decompose isopropanol with an excess of a radical scavenger (1,3,5-trimethylbenzene). They determined  $k_1$  by monitoring both the extent of decay of isopropanol and the extent of formation of propene between 979–1212 K and at pressures between 2.9–4.9 atm. Their  $k_1$  values were also larger than  $k_{1,\infty}$  from Bui *et al.*<sup>3</sup> by factors of 10–1.2 with the difference being smaller at higher temperatures. Cooper *et al.*<sup>13</sup> used time-resolved measurements of  $H_2O$  formation using laser absorption at 1.4 atm over a higher  $T$ -range, 1127–1621 K to also determine  $k_1$ . Simulations of the  $H_2O$  profiles were best-fit by the Li *et al.*<sup>11</sup> model and therefore these  $k_1$  values in the fall-off regime were also higher than the theoretical  $k_{1,\infty}$  predictions from Bui *et al.*

Despite the extant theoretical and experimental studies on the thermal decomposition processes in isopropanol, it is evident that there are no direct experimental studies for the kinetics of the key bond-fission process. Proper characterization of higher-energy bond-fissions in the presence of lower-energy molecular eliminations are known to be critical in high temperature decompositions.<sup>14–16</sup> We surmise that the observed discrepancies between the numerous literature studies are largely due to discrepancies in the kinetics for the bond-fission reaction (R2) since this serves as the rate-limiting step for radical driven secondary processes that rapidly break down reactants to intermediates. The present studies on isopropanol were therefore motivated by this lack of direct experimental kinetics on (R2).

## Methods

Two well established shock tubes equipped with optical diagnostics were used to study the early stages of isopropanol pyrolysis. The apparatuses and diagnostics have been previously described extensively and therefore only brief details are given below.

### Diaphragmless shock tube and laser schlieren densitometry

Laser schlieren (LS) densitometry<sup>17,18</sup> experiments were performed using a diaphragmless shock tube<sup>19,20</sup> (DFST). The driven section of the DFST is an electropolished 304 stainless-steel tube with an internal diameter of 6.35 cm. There is a pair of parallel quartz windows approximately 5.41 m downstream of the driver section. The driver section is made from 304 stainless-steel pipe and is similar to that shown in ref. 20. At the start of an experiment, a pneumatically actuated valve separated the driver and driven sections. The driven section was filled to pressure  $P_1$  with reagent mixture and the driver to pressure  $P_4$  with helium. Formation of the shock wave was initiated by rapidly opening the valve. The incident shock wave velocity was measured using five piezoelectric pressure transducers (Dynasen Model CA-1135) evenly spaced 120.0 mm apart and centered around the observation point. The temperature ( $T_2$ ) and pressure ( $P_2$ ) behind the incident shock wave were calculated from the measured shock wave velocity, initial conditions, ideal shock relations, and frozen chemistry assumptions. The uncertainty in the calculation of  $T_2$  and  $P_2$  is estimated to be  $\sim 0.5\%$  based on findings from past studies.

The LS experiments measure axial density gradients ( $d\rho/dx$ ) in the reacting gases within the DFST. This is done by measuring the deflection of a narrow continuous-wave laser beam (Thorlabs S1FC637, 637 nm) that traverses the DFST orthogonal to the direction of the incident shock wave. The deflection is measured by a quadrant photodiode (OSI SPOT-9DMI) which was configured to act as a two-segment diode with left and right halves. The angular deflection of the laser beam is proportional to the density gradient, the molar refractivity of the gas mixture, and the DFST internal diameter.<sup>17</sup> However, the density gradient is also proportional to the rate of reaction,  $R$ , and enthalpy



of reaction,  $\Delta H_r$ , summed over all reactions which allows kinetic and mechanistic information to be extracted from the measurements *via* eqn (1).

$$\frac{d\rho}{dx} \propto \sum_j R_j (\Delta H_{r,j} - CpT\Delta N_j) \quad (1)$$

$Cp$  is the constant-pressure heat capacity,  $T$  the temperature and  $\Delta N_j$  the change in mole number of the  $j$ th reaction. The term  $CpT\Delta N_j$  is typically about 10–15 kcal mol<sup>-1</sup>. Consequently, mildly endothermic reactions such as (R1) produce little measurable density gradients. However, such reactions must be accurately accounted for as they draw flux from other channels and may produce species that participate in reactions producing noticeable density gradients. The molar refractivity of krypton was obtained from Gardiner *et al.*<sup>21</sup> and that of isopropanol was calculated using the Lorenz–Lorentz equation with the molecular properties taken from Sigma Aldrich (density = 0.785 g mL<sup>-1</sup> at 25 °C; refractive index = 1.377). The typical assumption that the mixture molar refractivity for dilute mixtures, such as those used in this work, does not vary significantly with extent of reaction was made.

Fig. 1 shows an example of the measured (as-recorded) LS signal and the corresponding density gradients are shown in the inset figure. The large peak and preceding valley in the LS data at  $\sim 10 \mu\text{s}$  are due to shock front/laser beam interaction. On the right edge of the peak there is an abrupt change in slope, more clearly seen in the inset figure. Following this point in time, the LS signal is entirely due to chemical reactions in the shock-heated gases. The onset of reaction, indicated by  $t_0$  in Fig. 1 is obscured by the large peak and is located by a well-established method with an uncertainty of  $< 0.2 \mu\text{s}$ .<sup>17</sup> At  $t_0$ , dissociation of the reagent is the only reaction occurring. By simulating the density gradient profile, the density gradient at  $t_0$  can be obtained by extrapolation, and the total rate coefficient for dissociation of isopropanol can be determined.

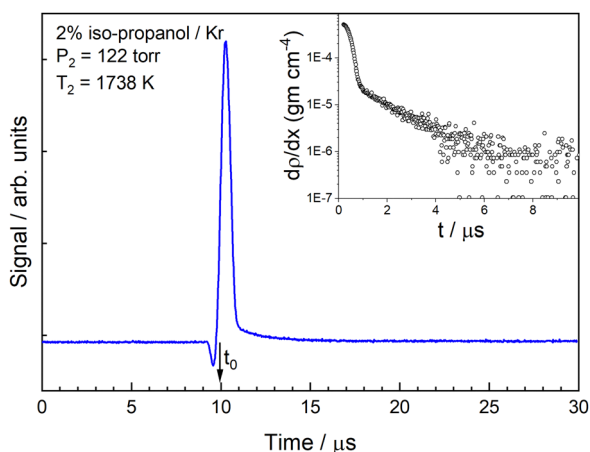


Fig. 1 Example LS signal (as-recorded). The approximate location of the onset of reaction,  $t_0$ , is indicated by the arrow. The inset shows the corresponding density gradient profile. The early steep portion of the density gradient time-history is due to shock front/laser beam interactions. The abrupt change in slope at  $\sim 0.75 \mu\text{s}$  and the following data are due to chemical reactions.

Mixtures were prepared manometrically in a pre-evacuated ( $\sim 10^{-5}$  torr) 50 L round-bottom flask. Mixtures were stirred for at least an hour with a magnetic stirrer prior to use. The initial concentrations of the gases studied were 1%, 2%, and 4% isopropanol dilute in krypton. The isopropanol was obtained from Sigma Aldrich (99.9%). Krypton 99.999% was obtained from Airgas. All species were used as supplied.

### Shock tube and H-atom resonance absorption spectroscopy (ST-ARAS)

The ST-ARAS experiments used Kr as the diluent with H-atom ARAS as the diagnostic.<sup>22</sup> The cylindrical 7 m long (3.75 cm i.d.) shock-tube driven section was constructed from 304 stainless steel tube, and the interior was honed to a mirror finish. The driven section was separated from the He driver chamber by a 4 mil unscored 1100-H18 aluminum diaphragm. Between experiments, the tube was routinely pumped (Edwards Vacuum Products Model CR100P) to lower than  $10^{-8}$  torr. Shock-wave velocities were measured with eight equally spaced pressure transducers (PCB Piezotronics, Inc., Model 113A21) mounted along the downstream part of the test section and recorded with a 4094C Nicolet digital oscilloscope. The temperature ( $T_5$ ) and density ( $\rho_5$ ) in the reflected shock-wave regime were calculated from this velocity. Corrections for boundary layer perturbations have been applied.<sup>23–25</sup> The oscilloscope was triggered by a pulse derived from the velocity gauge signal furthest from the diaphragm.

The photometer system was located 6 cm from the driven-section endplate. H-atom ARAS detection was used to follow  $[\text{H}]_t$ , the absolute H-atom concentrations as a function of time, quantitatively. The optical components (windows and lenses) were crystalline  $\text{MgF}_2$ , and the resonance lamp beam intensity (filtered through 4 cm of air (21%  $\text{O}_2$ ) at 1 atm to isolate the Lyman- $\alpha\text{H}$  wavelength at 121.6 nm) was measured by a Hamamatsu R8487 solar-blind photomultiplier tube, as described previously.<sup>26–29</sup> The atmospheric  $\text{O}_2$  filter serves as a monochromator since there is a narrow region of high transmittance in the  $\text{O}_2$  absorption spectrum at 121.6 nm. Signals were recorded with a LeCroy model LC334A oscilloscope which was triggered with the same pulse as the oscilloscope measuring the pressure transducer signals. For H-atom detection, the microwave driven resonance lamp was operated at 35 watts and 1.4 torr of research grade He (99.9999%) (effective Doppler temperature: 470 K).<sup>30</sup> Due to lamp gas hydrogeneous impurities in research grade He (even cooled with liquid  $\text{N}_2$ ), Lyman- $\alpha\text{H}$  radiation is emitted from the lamp along with a few percent of radiation that is extraneous (non-resonant). In order to measure the fraction of Lyman- $\alpha\text{H}$  present in the lamp, an  $\text{H}_2$  discharge flow system, an atom filter, is used to create large  $[\text{H}]$  ( $\sim 1 \times 10^{14}$  atoms  $\text{cm}^{-3}$ ) between the lamp and shock tube window<sup>26,30–32</sup> thereby removing all of the Lyman- $\alpha\text{H}$  in the emission lamp. It can be shown using line absorption theory<sup>26,30,33</sup> that  $[\text{H}] = 1 \times 10^{14}$  atoms  $\text{cm}^{-3}$  at room temperature will remove 99.6% of Lyman- $\alpha\text{H}$ . The fraction of non-resonant emission is  $\sim 10\%$ . This fraction is subtracted from

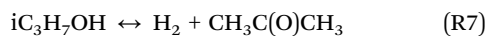
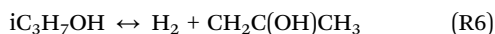
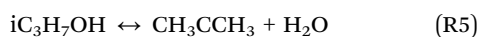


the measured photomultiplier-signal, meaning that 90% of the measured signal-intensity is Lyman- $\alpha$ H radiation.

High purity He (99.995%), used as the driver gas, was from AGA Gases. Research grade Kr (99.999%), the diluent gas in the reactant mixtures, was from Praxair, Inc. The  $\sim 10$  ppm impurities ( $N_2 < 5$  ppm,  $O_2 < 2$  ppm,  $Ar < 1$  ppm,  $CO_2 < 0.5$  ppm,  $H_2 < 1$  ppm,  $H_2O < 3$  ppm,  $Xe < 2$  ppm, and  $THC < 0.2$  ppm) are all either inert or in sufficiently low concentration to not perturb H-atom profiles. Isopropanol (99.9% purity) was obtained from Sigma-Aldrich. This was further purified by bulb-to-bulb distillation (in an all glass high-purity vacuum line) retaining only middle-thirds for mixture preparation. Gas mixtures of isopropanol ( $\sim 1$ – $2$  ppm) dilute in Kr were accurately prepared (using the same vacuum glass line) from pressure measurements using a Baratron capacitance manometer and stored in 22.4 L glass bulbs for subsequent use in the ST-ARAS studies reported here.

### Theory

Prior theoretical studies on isopropanol decomposition include the extensive calculations by Bui *et al.*<sup>3</sup> on the singlet potential energy surface (PES) at the G2M level of theory. Their calculations considered the three lowest energy bond-fissions that included C–C fission *via* (R2), tertiary C–H bond fission (R3), and C–OH bond fission (R4). Apart from these bond-fissions, they also calculated barrier heights for five additional molecular decompositions *via* reactions (R5)–(R9).



The lowest-lying channel was identified to be dehydration *via* (R1) with a calculated barrier height of 65.4 kcal mol<sup>-1</sup>. Aside from (R5) that had a barrier of 77.9 kcal mol<sup>-1</sup>, barriers for all other molecular decompositions ((R6)–(R9)) exceed 81 kcal mol<sup>-1</sup>. Bui *et al.* concluded that (R1) and (R2) were the only relevant channels in isopropanol decomposition from their theoretical kinetics predictions. Energy transfer though has a noticeable role to play with the theoretical work by Bui *et al.*<sup>3</sup> indicating that pressure fall-off is extensive in (R1) and (R2) at  $T > 1200$  K. The electronic structure theory calculations by Pokidova *et al.*<sup>6</sup> predict a much lower barrier of 61.97 kcal mol<sup>-1</sup> for (R1), and therefore their predicted rate coefficient at 800 K is orders of magnitude higher than the Bui *et al.* predictions. Buerger *et al.*<sup>7</sup> used the CBS-Q method but did not report the calculated barrier for (R1). To characterize the barrier-less reaction (R2) they used the VRC-TST method as implemented for alkyl radicals.<sup>34</sup> Buerger *et al.*<sup>7</sup> performed a master equation analysis and their predicted  $k_{1,\infty}$  was in reasonable agreement with the  $k_{1,\infty}$  predictions by Bui *et al.*

In this work, the rovibrational properties of the minima and transition states (of the molecular channels) for the important thermal decomposition steps in isopropanol were determined at the M06-2X/cc-pvtz level of theory. Higher level energy estimates for these stationary points were obtained using the CCSD(T)/cc-pV $\infty$ Z method where the infinite basis set limits are estimated from an extrapolation of results obtained from sequences of cc-pVnZ where  $n = (T,Q)$  basis sets.<sup>35,36</sup> Table S4 summarizes the energetics for the bond fissions and molecular channels in isopropanol at the CCSD(T)/cc-pV $\infty$ Z//M06-2X/cc-pvtz levels of theory. The predicted energetics in the present work differ by up to 2–3 kcal mol<sup>-1</sup> from the G2M calculations by Bui *et al.* However, the predicted barrier for the lowest-lying dehydration channel is  $\sim 0.5$  kcal mol<sup>-1</sup> higher in this work than that of Bui *et al.* while the bond-energy for (R2) is predicted to be 85.11 kcal mol<sup>-1</sup> ( $\sim 1.9$  kcal mol<sup>-1</sup> lower than the G2M prediction of 87 kcal mol<sup>-1</sup> from Bui *et al.*) in excellent agreement with the current ATcT recommendations (85.03 kcal mol<sup>-1</sup>).<sup>37</sup> One potentially relevant process that can confound the present analyses and was not considered in prior theoretical studies is roaming. Roaming pathways originating from (R2) can potentially lead to the formation of CH<sub>3</sub>CHO + CH<sub>4</sub> and CH<sub>2</sub>CHOH + CH<sub>4</sub>. However, a prior theoretical prediction<sup>38</sup> for roaming in ethanol indicates that this is a minor process ( $\sim 2\%$  of total reaction flux at 1300 K) and by analogy we assume that roaming will not compete with the two main channels, (R1) and (R2), in isopropanol dissociation at the conditions of this study.

Master equation calculations were performed with the VARIFLEX code using the present *ab initio* based energetics and molecular properties to obtain theoretical rate constants. The transition state partition functions were evaluated using phase space theory as implemented in VARIFLEX for (R2) whereas a conventional transition state theory treatment was employed for (R1). Sample calculations including higher energy molecular and radical processes indicated that these were negligible processes (over the  $T, P$  ranges of the present experiments), a conclusion also borne out by the Bui *et al.*<sup>3</sup> analyses. The coefficient for the inverse sixth power potential in the PST calculations was calibrated to match the capture rate constants for  $CH_3 + iso-C_3H_7$ <sup>34</sup> ( $\sim 2 \times 10^{-11}$  molecule cm<sup>-3</sup> s<sup>-1</sup>) for ( $T = 1000$ – $2500$  K) as an approximation to the  $CH_3 + CH_3CHOH$  capture rate. This analogy is reasonable as the calculations for the capture rate for  $CH_3 + CH_3CHOH$  by Buerger *et al.*<sup>7</sup> are in remarkably close agreement (within 7% over the 1000–2500 K  $T$ -range) with that of  $CH_3 + iso-C_3H_7$ .<sup>34</sup> 1-D hindered rotor treatments were employed for torsional modes, and tunnelling corrections using 1-d asymmetric Eckart barriers<sup>39–41</sup> were incorporated for (R1). Lennard-Jones parameters for Kr and estimates for isopropanol were taken from the literature.<sup>42,43</sup> Pressure dependent rate coefficients were calculated over the temperature range 1000–2500 K and fit to Arrhenius expressions that are presented in Table 1. The theoretical values and non-Arrhenius curve fits (and their errors) are available in the SI in tabular and graphical forms. An exponential down model was used for energy transfer with a temperature dependent



Table 1 Arrhenius fits to theoretical predictions for  $k_1$  and  $k_2$  ( $\text{s}^{-1}$ )

Pressure (atm)	A	n	$E_a/R$ (K)	Fit error
$k_1, 0.0395$	$1.00 \times 10^{75}$	-17.956	51 600	12%
$k_1, 0.0789$	$1.00 \times 10^{74}$	-17.612	51 600	9%
$k_1, 0.1579$	$1.00 \times 10^{73}$	-17.269	51 600	7%
$k_1, 0.3158$	$1.00 \times 10^{72}$	-16.927	51 600	6%
$k_1, 1.0$	$1.00 \times 10^{71}$	-16.527	52 100	9%
$k_1, 10$	$1.00 \times 10^{62}$	-13.826	50 000	12%
$k_1, 100$	$1.00 \times 10^{60}$	-13.010	51 500	17% <sup>a</sup>
$k_{1,\infty}$	$6.03 \times 10^8$	1.399	32 750	6%
$k_2, 0.0395$	$1.00 \times 10^{75}$	-17.640	54 400	13% <sup>a</sup>
$k_2, 0.0789$	$1.00 \times 10^{74}$	-17.262	54 400	15% <sup>a</sup>
$k_2, 0.1579$	$1.00 \times 10^{80}$	-18.786	57 600	17%
$k_2, 0.3158$	$1.00 \times 10^{79}$	-18.407	57 700	20%
$k_2, 1.0$	$1.00 \times 10^{78}$	-17.958	58 250	13% <sup>a</sup>
$k_2, 10$	$1.00 \times 10^{77}$	-17.328	60 150	13%
$k_2, 100$	$1.00 \times 10^{75}$	-16.436	61 900	15%
$k_{2,\infty}$	$3.96 \times 10^{24}$	-2.076	45 000	1%

Fits valid between 1000–2500 K except <sup>a</sup> which are valid between 1100–2500 K.

$\langle \Delta E_{\text{down}} \rangle = 150 (T/298)^{0.85} \text{ cm}^{-1}$ , which is a reasonable estimate,<sup>44</sup> and this allowed comparisons with the experimentally determined rate coefficients from the present shock tube studies that span pressures from 0.08–0.91 atm over the extended temperature range 1196–2090 K.

### Elementary reaction mechanism and modelling approach

The density gradient profiles behind the incident shock wave from the LS experiments were simulated using the chemical kinetic mechanism presented here and the computer program Frhodo.<sup>45</sup> The same mechanism was used to simulate the H-ARAS experiments which were modelled as a 0D constant volume homogeneous reactor using the ANSYS Chemkin package.<sup>46</sup>

The reactions for pyrolysis of isopropanol (unimolecular and bimolecular reactions) are shown in Table S1 of the SI. The initial values for  $k_1$  and  $k_2$  were taken from the master equation results. Rate coefficients for H attack on isopropanol resulting in abstraction of a hydrogen atom were set to the values calculated in this work. Those for abstraction by  $\text{CH}_3$  were taken from Saggese *et al.*,<sup>47</sup> and those involving OH radical were from Guo *et al.*<sup>48</sup> In this study, the OH and  $\text{CH}_3$  initiated reactions were of minor importance relative to those initiated by H-atoms.

The ThInK 1.0 mechanism<sup>49,50</sup> was used as the base chemistry mechanism. ThInK 1.0 is a theory informed kinetics model which has been developed over several years. The model includes *a priori* high-level theoretical predictions for the elementary reactions as well as thermochemistry and transport parameters for species involved in small molecule combustion chemistry ( $\text{H}_2$  and C0–C3 species). The first principles-based approaches have been described in recent reviews by the model's authors.<sup>51,52</sup> The methods used enable the creation of reaction mechanisms that rely on theory alone, yet possess predictive power over wider temperature, pressure, and concentration ranges than prior approaches. A preliminary version of this mechanism and limited simulations were presented in prior work.<sup>53</sup> The current version of the model<sup>49,50</sup> makes

reliable predictions of the extant literature data on auto-ignition and laminar flame propagation for the core combustion species.

The reactions involving and deriving from isopropanol were added to ThInK 1.0, which includes the chemistry for all the subsequent species produced from the unimolecular initiations (R1) and (R2), and bimolecular H-abstraction reactions from isopropanol. Of relevance here are the kinetics for the  $\text{C}_3\text{H}_7\text{O}$  radicals for which ThInK relies on the theoretical predictions from Zador *et al.*<sup>54</sup> Additional reactions added to the ThInK mechanism included a better description of the chemistry of acetone and for this we relied on the theoretical predictions from Zaleski *et al.*<sup>55</sup> Details of these are given in Table S1. The complete model and thermochemistry are provided in the SI. Details of these are given in Table S1 and is also provided as a Chemkin compatible kinetics model in the SI.

## Results

### ST-ARAS

Thirty-three experiments were performed behind reflected shock waves over the temperature range 1195–1509 K and at nominal pressures of 0.2, 0.48, and 0.86 atm (150, 365 and 655 torr). Unimolecular dissociation of isopropanol does not directly produce H-atoms. However,  $\text{CH}_3\text{CHOH}$  (formed in (R2)) nearly instantaneously decomposes to produce H-atoms *via* two competing reactions, (R10) and (R11).



In the absence of reactions that deplete  $[\text{H}]$ , the results will then be direct measures for the kinetics of reactions (R1) and (R2). Fig. 2 shows typical H-atom profiles at  $T = 1253$  K using  $[\text{isopropanol}]_0 = 1.102 \times 10^{13} \text{ molecules cm}^{-3}$  (2.16 ppm), and 1467 K using  $[\text{isopropanol}]_0 = 1.141 \times 10^{12} \text{ molecules cm}^{-3}$  (1.06 ppm). If the sensitivity for H-detection is high, secondary reaction perturbations become negligible, and then the temporal behavior is only dependent on these two primary initiation channels. Under such scenarios, the rate of formation of H-atoms can be simulated by applying a simple first-order analysis leading to eqn (2) where  $[\text{isopropanol}]_0$  is the initial concentration of isopropanol and  $t$  is time.

$$[\text{H}]_t = (k_2[\text{isopropanol}]_0 / (k_1 + k_2)) \times (1 - \exp(-(k_1 + k_2)t)) \quad (2)$$

This first-order analysis was used to obtain preliminary values for  $k_1$  and  $k_2$ . The solid line shown in Fig. 2 was determined from the full mechanism presented here. To obtain the final  $k_2$  values both  $k_1$  and  $k_2$  were adjusted manually to obtain the best fit for each experiment. Sensitivity analyses for the two  $[\text{H}]_t$  profiles depicted in Fig. 2 are shown in Fig. 3, where it is evident that the H-atom formation at early-times depends only on  $k_2$ . The high sensitivity of the H-ARAS setup (detection limit  $< 5 \times 10^{10}$  atoms per cc) means that  $[\text{isopropanol}]_0$  of 1–2 ppm could be used, thereby effectively



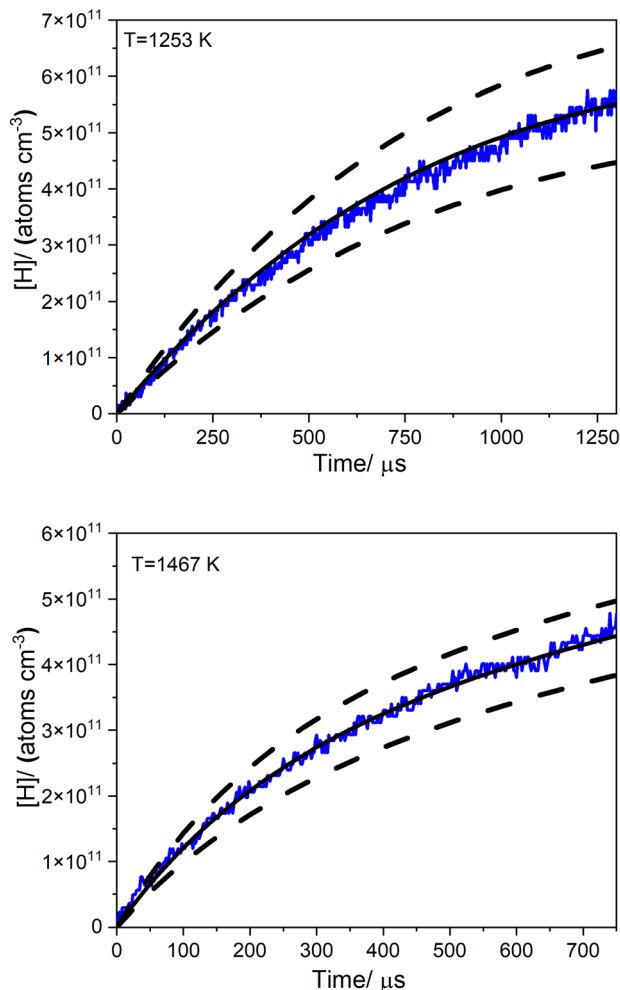


**Fig. 2**  $[H]_t$  profiles (shown in blue) from isopropanol decomposition at 1253 K and 1467 K. The solid black line is a fit over the entire time range using the present model. The dashed lines represent changes in the best-fit  $k_2$  values by  $\pm 20\%$ . The conditions for the experiment at  $T_5 = 1253$  K are  $P_2 = 30.75$  torr, Mach number ( $M_5$ ) = 2.228,  $\rho_5 = 5.106 \times 10^{18}$  molecules  $\text{cm}^{-3}$ , and  $[\text{isopropanol}]_0 = 1.102 \times 10^{13}$  molecules  $\text{cm}^{-3}$ . The conditions for the experiment at  $T_5 = 1467$  K are  $P_2 = 5.81$  torr,  $M_5 = 2.417$ ,  $\rho_5 = 1.079 \times 10^{18}$  molecules  $\text{cm}^{-3}$ , and  $[\text{isopropanol}]_0 = 1.141 \times 10^{12}$  molecules  $\text{cm}^{-3}$ .

suppressing bimolecular reactions at short reaction times. At longer-times and  $T < 1300$  K, the only reaction other than (R2) that is sensitive is (R1). In prior studies *e.g.* ref. 56, where the reactant was fully consumed, the  $[H]_t$  profiles attained a constant maximum value at long-times. Applying a first-order analysis in such scenarios enables direct measurements of not just total rate coefficients for reactant loss, but also direct branching ratios for the H-atom forming channel. This facilitates direct determinations of rate coefficients<sup>56</sup> for two-channel thermal unimolecular dissociation processes where only one channel exclusively forms H-atoms. However, in the present studies at  $T < 1300$  K, complete depletion of reactants did not occur in the  $\sim 2$  ms observation time. Furthermore, at higher- $T$  where consumption was complete, decompositions of the products from (R1) and (R2) by reaction (R12)–(R14) also produced H-atoms.

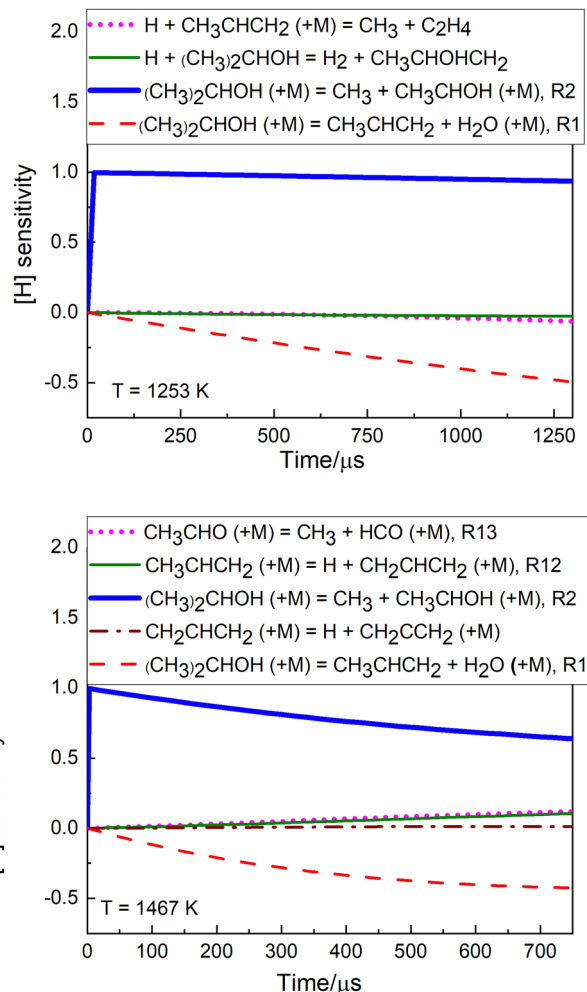
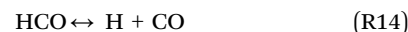
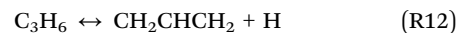


**Fig. 3**  $[H]_t$  sensitivity analyses for the experiments shown in Fig. 2 using the best-fit  $k_2$  values used in the mechanism. Reaction numbers correspond to the text. Reactions that are not numbered appear only in the mechanism in the SI.



Consequently, the long-time  $[H]_t$  profiles include contributions from these reactions and therefore do not allow the direct application of first-order analysis to determine branching ratios as in prior studies.<sup>56</sup> However, (R12)–(R14) are all well-characterized and the sensitivity analyses show that they have a negligible impact on the determined  $k_2$  values. The final best-fit values for  $k_2$  using the detailed mechanism were within  $\pm 20\%$  of the preliminary  $k_2$  values from the first-order analyses (eqn (2)). This is also reflected in the simulations represented by the dashed lines in Fig. 2, where changes to  $k_2$  by  $\pm 20\%$  significantly degrade the fits to the  $[H]_t$  profiles. The best-fit  $k_2$  values for each experiment are presented in Table S2 in the SI. Arrhenius fits to the first order rate coefficients (see SI) for  $k_2$  from the H-ARAS experiments lead to



$$k_2 = 7.00 \times 10^{10} \exp(-25760K/T) \text{ s}^{-1} \quad (0.2 \text{ atm}, 1318\text{--}1509 \text{ K}) \quad (3)$$

$$k_2 = 3.28 \times 10^{11} \exp(-27879K/T) \text{ s}^{-1} \quad (0.48 \text{ atm}, 1240\text{--}1350 \text{ K}) \quad (4)$$

$$k_2 = 9.00 \times 10^{13} \exp(-34860K/T) \text{ s}^{-1} \quad (0.86 \text{ atm}, 1195\text{--}1292 \text{ K}) \quad (5)$$

These expressions are valid only over the listed ranges and should not be extrapolated to other conditions.

### DFST/LS

One hundred and nineteen LS experiments were conducted behind incident shock waves at temperatures from 1550 to 2100 K and nominal pressures of 30, 60, 120, and 250 torr. A summary of the experiments is provided in Table 2 with details of the experimental conditions and rate coefficients tabulated in Table S3 in the SI. Typical density gradient profiles from isopropanol laser schlieren experiments using 2% and 4% isopropanol are presented for two state conditions in Fig. 4. The density gradients remain positive throughout the observation period, indicating endothermic reactions dominate and that radical recombination reactions, typically strongly exothermic, are of minor importance in the short observation period.

In Fig. 4, absolute values of the density gradients are plotted and results from two simulations are compared with an experiment. The solid line depicts results obtained with the final mechanism presented here. The broken line represents the current model, but with  $k_1$  and  $k_2$  replaced by the corresponding values from Li *et al.*<sup>11</sup> The simulations with the Li *et al.* values consistently overpredict consumption of isopropanol and secondary reactions quickly force the simulated density gradients lower than the experimental values. Furthermore, the simulations quickly produce net negative density gradients contrary to the experimental observations. Simulations with the complete mechanism from Li *et al.* produce similar results.

Similar to the H-ARAS studies,  $k_1$  and  $k_2$ , were iteratively adjusted for each experiment to visually obtain the best fit at early times ( $< 4 \mu\text{s}$ ) between the experiment and simulation results. The simulated density gradient profiles were sensitive to the rate of dissociation of isopropanol and the branching fraction between the (R1) and (R2). Due to the low endothermicity of (R1) (12.1 kcal mol<sup>-1</sup>) and the large endothermicity of (R2) (85.1 kcal mol<sup>-1</sup>) the simulations were most sensitive to  $k_2$ . Consequently,  $k_1$  was initially set to the theoretical values and for a few experiments  $k_1$  was adjusted by up to a factor of 1.2, whereas  $k_2$  was varied to best fit the early-time density gradients. Fig. 5 shows the sensitivity of the simulations to variation

Table 2 LS experimental conditions studied

Pressure (torr)	Temperature (K)	Isopropanol concentration (mole basis in Kr)
250	1497–1941	2%
120	1478–2082	1%, 2%, 4%
60	1608–2035	2%, 4%
30	1636–2090	2%, 4%

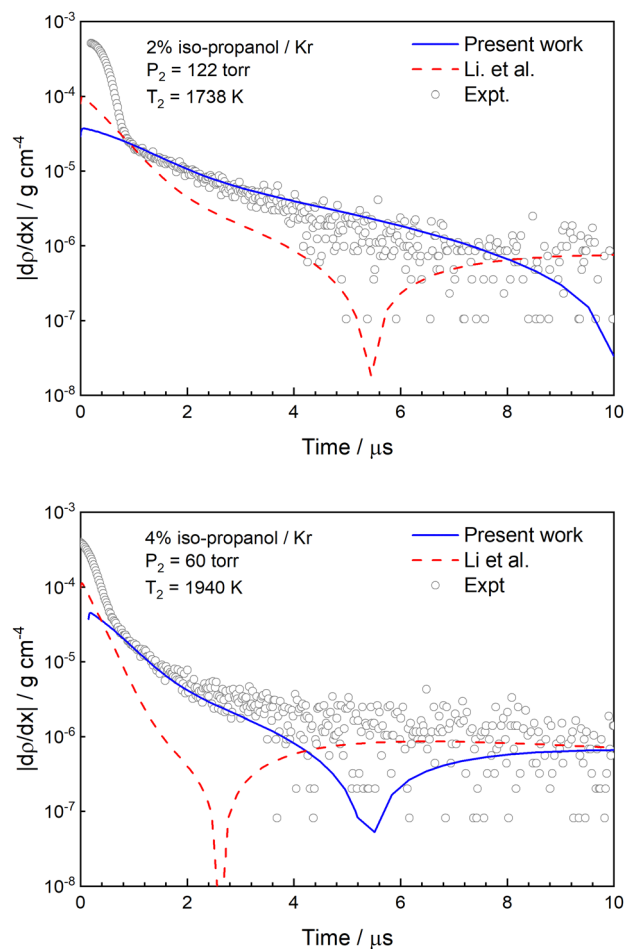


Fig. 4 Typical experimental results (symbols) for absolute density gradients and comparison with model predictions (lines). The solid lines represent simulations using the current model.  $k_1$  and  $k_2$  were replaced with values from Li *et al.*<sup>11</sup> to generate the dashed lines.

in  $k_2$  by a factor of 2. For the majority of the experiments  $k_2$  was adjusted by  $< 50\%$  from the initial value. (R1), the water elimination channel, must be accurately accounted for because it draws flux away from (R2) and secondary reactions of propene produced by (R1) are important, especially at high temperatures. Arrhenius fits to the first order rate coefficients (see SI) for  $k_2$  from the LS experiments at 30, 60, 120, and 250 torr lead to,

$$k_{2,30\text{torr}} = 1.26 \times 10^{14} \text{ T}^{-1.32} \exp(-22500K/T) \text{ s}^{-1} \quad (1636\text{--}2090 \text{ K}) \quad (6)$$

$$k_{2,60\text{torr}} = 1.64 \times 10^{29} \text{ T}^{-5.50} \exp(28110K/T) \text{ s}^{-1} \quad (1608\text{--}2035 \text{ K}) \quad (7)$$

$$k_{2,120\text{torr}} = 1.93 \times 10^{46} \text{ T}^{-10.19} \exp(-34860K/T) \text{ s}^{-1} \quad (1478\text{--}2082 \text{ K}) \quad (8)$$

$$k_{2,250\text{torr}} = 1.00 \times 10^{47} \text{ T}^{-10.27} \exp(-35801K/T) \text{ s}^{-1} \quad (1497\text{--}1941 \text{ K}) \quad (9)$$

that are valid only over the listed pressure and temperature ranges and should not be extrapolated to other conditions. At



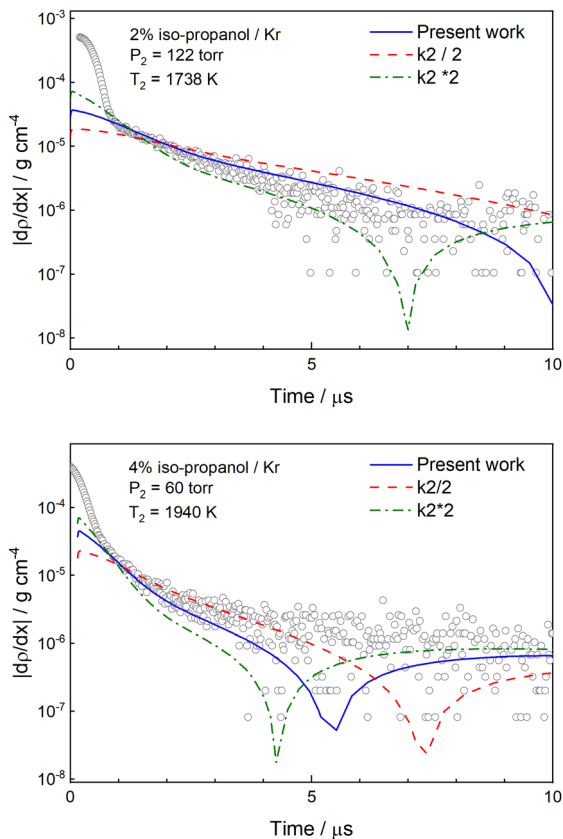
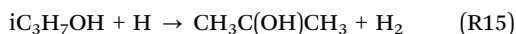


Fig. 5 Plots of absolute density gradients showing the sensitivity of the LS simulations to variations of a factor of 2 in  $k_2$ ,  $iC_3H_7OH \rightarrow CH_3 + CH_3CHOH$ .

higher temperatures and/or longer times the simulated gradients show a sharp dip indicating that the net density gradient has become negative. This is primarily due to a set of reactions initiated by  $CH_3C(OH)CH_3$ , which is produced by abstraction of the tertiary hydrogen from isopropanol in (R15)



## Discussion

Cumulatively, the experimental measurements for  $k_2$  from the two shock-tube studies span an extensive temperature range, 1195–2090 K and pressure range, 0.04–0.9 atm, thereby providing a rigorous test for pressure fall-off in this dominant bond-fission channel. Fig. 6 depicts the experimental results (shown as symbols for both the ARAS and LS studies) with the present theoretical predictions (depicted by lines) providing a comprehensive description of  $k_2(T, P)$ . It is evident the extent of fall-off in this bond-fission is severe as indicated by both the measurements and theory. Specifically,  $k_2$  values at 1 atm are an order of magnitude less than the value of  $k_{2,\infty}$  at 1500 K, with larger deviations observed with increasing temperatures. In the absence of prior direct measurements, comparisons of the theoretical predictions in this study with the prior theoretical

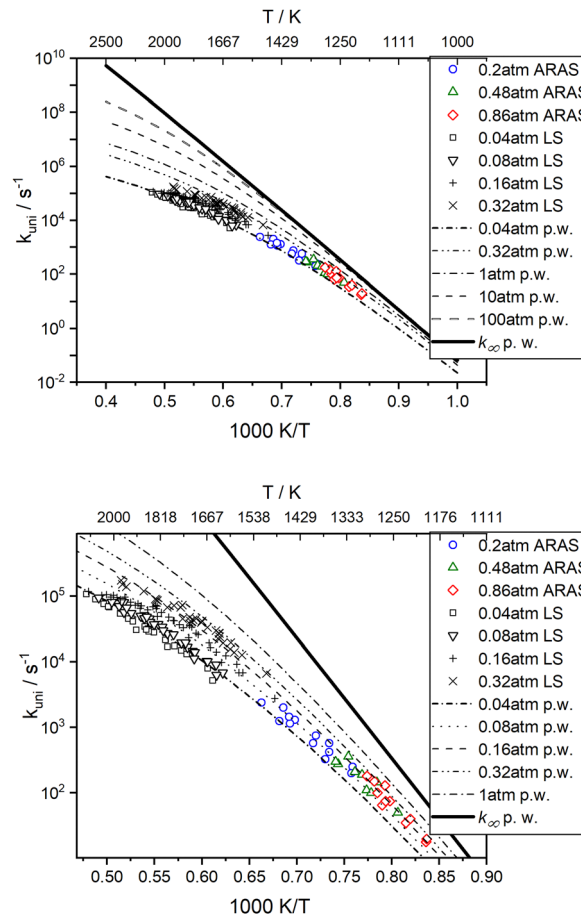


Fig. 6 Fall-off first-order Arrhenius results for  $k_2$ . Color symbols are  $k_2$  from ARAS experiments; Black symbols are  $k_2$  from LS experiments; Lines are theoretical predictions from this work. The lower plot is zoomed to the experimental data.

predictions from Bui *et al.* are depicted in Fig. S1 in the SI. While there is a reasonable agreement in predicted  $k_{2,\infty}$  values between the two studies, the predicted extent of fall-off is more severe in the Bui *et al.* predictions. This is in quantitative disagreement with the present experimental measurements and theory; for example, the 50 torr Bui *et al.* predictions at  $T > 1500$  K are approximately a factor of two lower than the present 30 torr (0.04 atm) data and predictions.

Buerger *et al.*<sup>7</sup> have also provided  $k_2(T, P)$  fits, and comparisons with the fits from Buerger *et al.*<sup>7</sup> indicate much lower  $k_{2,\infty}$  than that of Bui *et al.* (by a factor of 3 at 1500 K) and the present theoretical predictions (by a factor of 5 at 1500 K). It is therefore not surprising to observe that the Buerger *et al.* 1 atm predictions for  $k_2$  are lower than even the 0.04 atm predictions and experiments from the present work. The small differences (factors of 2–3) between the present predictions and that from Bui *et al.* are attributed to the differences in barriers, molecular properties, and the choice of energy transfer parameters. However, in the absence of any details about the kinetics predictions in the Buerger *et al.*<sup>7</sup> work, the sources for the larger discrepancies between their predictions and that of Bui *et al.*<sup>3</sup> and the current work cannot be ascertained.



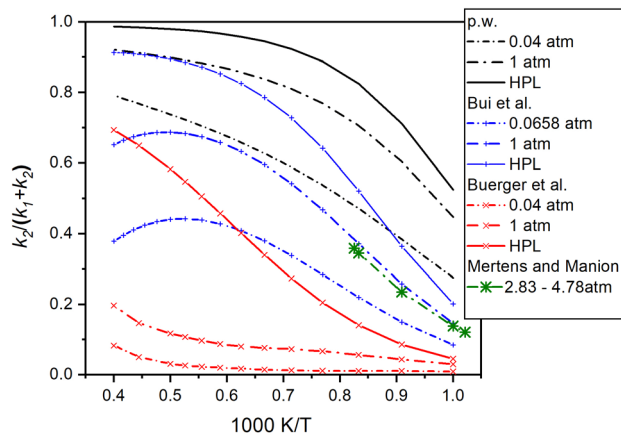


Fig. 7 Comparison of branching ratios (BR) for isopropanol decomposition. Black lines – theoretical predictions from the present work (p.w.), blue lines with + symbols – Bui *et al.*,<sup>3</sup> red lines with x symbols – Buerger *et al.*,<sup>7</sup> green line with \* – Mertens and Manion<sup>12</sup> estimates. HPL = BR at the high pressure limit.

Another set of comparisons were made between the present predictions and the analogy-based estimates from Li *et al.*<sup>11</sup> and the optimization derived values from Mertens and Manion<sup>12</sup> (over a limited temperature and pressure range) are depicted in Fig. S2 in the SI. At  $T < 1500$  K, at the lowest pressures (30 torr) the estimates in the Li *et al.* model are factors of 3–4 larger than the present predictions. At higher pressures, the differences are factors of 2–3. It is evident that the estimates for  $k_2(T, P)$  that are based on C–C fission for *n*-butanol in the Li *et al.* model do not match the present theoretical predictions (and experimental data) for the extent of fall-off in (R2). On the other hand, the results based on optimization from Mertens and Manion that are valid over a narrow range of pressures (2.8–4.7 atm) and temperatures (1000–1200 K) are within 10% of the present predictions at 1 atm. Under these conditions, theory predicts that fall-off is not as severe with  $k_{2,1\text{atm}}(1200\text{ K}) \sim 0.37k_{2,\infty}(1200\text{ K})$ . As discussed below, this is crucial in interpreting the majority of high-temperature experiments on isopropanol since (R2) provides an initial source for reactive radicals.

While the present experimental studies have largely isolated the kinetics for (R2), it is also useful to compare branching ratios between (R1) and (R2) from the present theoretical predictions with the literature studies. The detailed analysis by Mertens and Manion concludes that studies in the literature at lower temperatures using flow/static reactors<sup>5,8</sup> can be impacted by radical chain reactions in experiments that are not completely inhibited by free-radical scavengers. This places an emphasis not only on  $k_2$  values, but also on the branching between the two main reactions of interest in isopropanol decomposition.

Fig. 7 depicts the branching ratios for  $k_{R2}$  relative to  $(k_{R1} + k_{R2})$  from the present theoretical predictions as well as literature predictions<sup>3,7</sup> and estimates.<sup>12</sup> There are noticeable differences between the predicted branching ratios for the radical channel (R2) from the current work and the two prior

theoretical predictions and the estimates from Mertens and Manion. The predictions from the present work indicate the radical channel is dominant at  $T > 1200$  K at  $P > 30$  torr. This is in significant discrepancy with the modelling by Bui *et al.*<sup>3</sup> that predicts the dominance of the radical channel only at  $T > 1300$  K for  $P > 1$  atm. The Buerger *et al.*<sup>7</sup> study under-predicts the branching to radical products even more severely, with (R2) dominating only at  $T > 1800$  K at the high-pressure limit. The estimates derived by the optimization study from Mertens and Manion<sup>12</sup> also underpredicts the branching to radical products (relative to the present work) and is in closer agreement with the Bui *et al.*<sup>3</sup> predictions.

The Buerger *et al.* predictions for the radical channel seem to be anomalously low if one were to draw analogies with branching to the C–C fission in ethanol. In prior studies by Sivaramakrishnan *et al.*,<sup>15</sup> theoretical predictions were in excellent agreement with the direct experimental measurements for the branching ratios in ethanol. Comparisons of the theoretical predictions from this earlier study<sup>15</sup> at 1 atm indicated that branching to C–C fission in ethanol was even larger than the Buerger *et al.*<sup>7</sup> 1 atm branching ratios to (R2) in isopropanol. Lastly, the recent study on isopropanol decomposition using a laser diagnostic for H<sub>2</sub>O by Cooper *et al.*<sup>13</sup> relied on the Li *et al.*<sup>11</sup> model for their simulations.

As discussed earlier, not only are there discrepancies between the  $k_2(T, P)$  values from Li *et al.* and the present predictions, but the discrepancies are even larger for  $k_1(T, P)$ . Branching to dehydration is more favored in the Li *et al.* model than the present predictions. Consequently, simulations (see SI) of the Cooper *et al.* data with the model used in the present work indicates that H<sub>2</sub>O formation in these experiments are not sensitive to  $k_1$  but instead are sensitive to secondary reactions catalyzed by radicals from the dominant initiation reaction (R2). It can therefore be hypothesized that using radical scavengers cannot completely suppress radical reactions in most of the literature experiments at  $P \geq 1$  atm given the dominance of (R2) at  $T > 1000$  K. A brief discussion on the impact of the present results on Merten and Manion's experiments is given in the SI. As exemplified in recent studies by Cho *et al.*,<sup>16</sup> the present work again emphasizes the key role of branching to radical processes in multi-channel thermal decompositions.

## Conclusions

The initial decomposition processes in isopropanol were investigated with two complementary shock-tube techniques, one a diaphragmless shock tube using laser-schlieren densitometry, and the other a shock tube with atomic resonance absorption spectroscopy. More than 150 shock tube experiments were performed using the two methods over an extended range of temperatures and pressures spanning 1200–2100 K and 30–690 torr. High-level theoretical calculations were used to predict the pressure and temperature dependent rate coefficients for the two primary isopropanol decomposition reactions forming



water, (R1), and radicals, (R2). Simulations of the two shock-tube data sets using a kinetics model were used to unambiguously determine high temperature kinetics [ $k_2(T, P)$ ] for the C–C fission in isopropanol. The theoretical predictions are in good agreement with the experimental  $k_2(T, P)$  values that span the fall-off regime and therefore provide reliable extrapolations to a wider-range of pressures and temperatures. Fits to the theoretical  $k_2(T, P)$  values are presented in Table 1 and in the model in the SI for use in practical simulations. The present experiments and theory indicate the  $k_2(T, P)$  values and branching to (R2) is under-predicted in prior literature studies, and therefore re-interpretation of prior studies that focussed on the kinetics of the dehydration channel (R1) at high temperatures might be warranted.

## Author contributions

J. H. Kim: investigation, data curation, visualization, writing – original draft. K. Kim: investigation. R. Sivaramakrishnan: conceptualization, investigation, data curation, supervision, writing. S. Peukert: investigation. J. V. Michael: conceptualization, supervision, investigation. M. S. Wooldridge: investigation, supervision, writing – review & editing. R. S. Tranter: conceptualization, investigation, data curation, supervision, writing – review & editing.

## Conflicts of interest

There are no conflicts to declare.

## Data availability

The data supporting this article have been included as part of the SI. The SI: Fits to the theoretical  $k_1$  and  $k_2$ ; a Chemkin style file with the thermochemistry, rate coefficient expressions and reactions for pyrolysis of isopropanol; plots comparing  $k_1$  and  $k_2$  with literature values; tables of data from the shock tube experiments; energetics for the potential energy surface for isopropanol dissociation; a table of molecular structures and frequencies. See DOI: <https://doi.org/10.1039/d5cp02482j>

## Acknowledgements

This material is based on work supported by the U.S. Department of Energy, Office of Basic Energy Sciences, Division of Chemical Sciences, Geosciences, and Biosciences through Argonne National Laboratory. Argonne is a U.S. Department of Energy laboratory managed by UChicago Argonne, LLC, under contract DE-AC02-06CH11357. JHW was supported by the U.S. Department of Energy, Office of Science, Office of Workforce Development for Teachers and Scientists, Office of Science Graduate Student Research (SCGSR) program. The SCGSR program is administered by the Oak Ridge Institute for Science and Education (ORISE) for the DOE. ORISE is managed by ORAU under contract number DE-SC0014664.

All opinions expressed in this paper are the authors' and do not necessarily reflect the policies and views of DOE, ORAU, or ORISE.

## References

- 1 M. A. Burnett, J. Kim, S. W. Wagon, A. B. Mansfield and M. S. Wooldridge, *J. Phys. Chem. A*, 2022, **126**, 9097–9107.
- 2 J. H. Kim, K. Kim, Q. Meng, A. Sutar, M. S. Wooldridge and R. S. Tranter, *Phys. Chem. Chem. Phys.*, 2025, **27**, 7409–7420.
- 3 B. H. Bui, R. S. Zhu and M. C. Lin, *J. Chem. Phys.*, 2002, **117**, 11188–11195.
- 4 W. Tsang, *Int. J. Chem. Kinet.*, 1976, **8**, 173–192.
- 5 A. B. Trenwith, *J. Chem. Soc., Faraday Trans. 1*, 1975, **71**, 2405–2412.
- 6 T. S. Pokidova, E. T. Denisov and A. F. Shestakov, *Pet. Chem.*, 2009, **49**, 343–353.
- 7 P. Buerger, D. Nurkowski, J. Akroyd and M. Kraft, *Proc. Combust. Inst.*, 2017, **36**, 1019–1027.
- 8 J. S. Heyne, S. Dooley, Z. Serinyel, F. L. Dryer and H. Curran, *Z. Phys. Chem.*, 2015, **229**, 881–907.
- 9 C. M. Rosado-Reyes, W. Tsang, I. M. Alecu, S. S. Merchant and W. H. Green, *J. Phys. Chem. A*, 2013, **117**, 6724–6736.
- 10 S. Jouzdani, A. Zhou and B. Akih-Kumgeh, *Combust. Flame*, 2017, **176**, 229–244.
- 11 W. Li, Y. Zhang, B. Mei, Y. Li, C. Cao, J. Zou, J. Yang and Z. Cheng, *Combust. Flame*, 2019, **207**, 171–185.
- 12 L. A. Mertens and J. A. Manion, *Int. J. Chem. Kinet.*, 2021, **53**, 95–126.
- 13 S. P. Cooper, C. R. Mulvihill, O. Mathieu and E. L. Petersen, *Int. J. Chem. Kinet.*, 2021, **53**, 536–547.
- 14 S. L. Peukert, R. Sivaramakrishnan, M.-C. Su and J. V. Michael, *Combust. Flame*, 2012, **159**, 2312–2323.
- 15 R. Sivaramakrishnan, M. C. Su, J. V. Michael, S. J. Klippenstein, L. B. Harding and B. Ruscic, *J. Phys. Chem. A*, 2010, **114**, 9425–9439.
- 16 J. Cho, N. J. Labbe, L. B. Harding, S. J. Klippenstein and R. Sivaramakrishnan, *Proc. Combust. Inst.*, 2024, **40**, 105684.
- 17 J. H. Kiefer, in *Shock Waves in Chemistry*, ed. M. Dekker, New York, 1981.
- 18 J. H. Kiefer, M. Z. Al-Alami and J. C. Hajduk, *Appl. Opt.*, 1981, **20**, 221–230.
- 19 R. S. Tranter and B. R. Giri, *Rev. Sci. Instrum.*, 2008, **79**, 094103.
- 20 J. B. Randazzo and R. S. Tranter, *Rev. Sci. Instrum.*, 2015, **86**, 016117.
- 21 W. C. Gardiner, Y. Hidaka and T. Tanzawa, *Combust. Flame*, 1981, **40**, 213–219.
- 22 J. V. Michael, *Prog. Energy Combust. Sci.*, 1992, **18**, 327–347.
- 23 J. V. Michael and J. W. Sutherland, *Int. J. Chem. Kinet.*, 1986, **18**, 409–436.
- 24 J. V. Michael, *J. Chem. Phys.*, 1989, **90**, 189–198.
- 25 J. V. Michael and J. R. Fisher, Seventeenth International Symposium on Shock Waves and Shock Tubes, AIP Conference Proceedings 208, New York, 1990.



- 26 J. V. Michael and A. Lifshitz, in *Handbook of Shock Waves*, ed. G. Ben-Dor, O. Igra and T. O. V. Elperin, Academic Press, Burlington, 2001, pp. 77–105.
- 27 S. S. Kumaran, J. J. Carroll and J. V. Michael, *Proc. Combust. Symp.*, 1998, **27**, 125–133.
- 28 K. P. Kim and J. V. Michael, *Proc. Combust. Symp.*, 1994, **25**, 713–719.
- 29 S. S. Kumaran, M. C. Su, K. P. Lim and J. V. Michael, *Proc. Combust. Symp.*, 1996, **26**, 605–611.
- 30 R. G. Maki, J. V. Michael and J. W. Sutherland, *J. Phys. Chem.*, 1985, **89**, 4815–4821.
- 31 S. L. Mielke, K. A. Peterson, D. W. Schwenke, B. C. Garrett, D. G. Truhlar, J. V. Michael, M.-C. Su and J. W. Sutherland, *Phys. Rev. Lett.*, 2003, **91**, 063201.
- 32 J. V. Michael, M. C. Su, J. W. Sutherland, L. B. Harding and A. F. Wagner, *Proc. Combust. Inst.*, 2005, **30**, 965–973.
- 33 A. C. G. Mitchell and N. W. Zernansky, *Resonance Radiation and Excited States*, Cambridge University Press, Cambridge, England, 1934.
- 34 S. J. Klippenstein, Y. Georgievskii and L. B. Harding, *Phys. Chem. Chem. Phys.*, 2006, **8**, 1133–1147.
- 35 J. M. L. Martin, *Chem. Phys. Lett.*, 1996, **259**, 669–678.
- 36 J. A. Miller and S. J. Klippenstein, *J. Phys. Chem. A*, 2003, **107**, 2680–2692.
- 37 D. H. Bross and B. Ruscic, *Active Thermochemical Tables (ATcT) values based on ver. 1.220 of the Thermochemical Network*, Argonne National Laboratory, Lemont, Illinois, USA, 2025; available at ATcT.anl.gov.
- 38 A. G. Vandeputte, L. B. Harding, Y. Georgievskii and S. J. Klippenstein, 8th US National Combustion Meeting, Park City, UT, 2013.
- 39 C. Eckart, *Phys. Rev.*, 1930, **35**, 1303–1309.
- 40 H. S. Johnston, *Gas Phase Reaction Rate Theory*, Ronald Press, New York, 1966.
- 41 B. C. Garrett and D. G. Truhlar, *J. Phys. Chem.*, 1979, **83**, 2921–2926.
- 42 J. O. Hirschfelder, C. F. Curtiss and R. B. Bird, *The Molecular Theory of Gases and Liquids*, John Wiley, New York, 1964.
- 43 B. E. Poling, J. M. Prausnitz and J. P. O. Connell, *The Properties of Gases and Liquids*, McGraw-Hill, New York, 2001.
- 44 J. A. Miller and S. J. Klippenstein, *Phys. Chem. Chem. Phys.*, 2004, **6**, 1192–1202.
- 45 T. Sikes and R. S. Tranter, *Combust. Flame*, 2023, **257**, 112509.
- 46 ANSYS Chemkin 2022 R1 (29-Nov-2021). Copyright©2022 ANSYS, Inc.
- 47 C. Saggese, C. M. Thomas, S. W. Wagnon, G. Kukkadapu, S. Cheng, D. Kang, S. S. Goldsborough and W. J. Pitz, *Proc. Combust. Inst.*, 2021, **38**, 415–423.
- 48 X. Guo, R. M. Zhang, L. G. Gao, X. Zhang and X. Xu, *Phys. Chem. Chem. Phys.*, 2019, **21**, 24458–24468.
- 49 S. J. Klippenstein, R. Sivaramakrishnan, N. J. Labbe, Y. Tao, M. P. Burke, S. N. Elliott, C. F. Goldsmith, C. R. Mulvihill, A. W. Jasper, B. Ruscic, D. H. Bross, P. Glarborg, N. Hansen, J. Zador and J. A. Miller, *Combust. Flame*, 2025, in review.
- 50 R. Sivaramakrishnan, D. H. Bross, M. P. Burke, S. N. Elliot, P. Glarborg, C. F. Goldsmith, N. Hansen, A. W. Jasper, N. J. Labbe, J. A. Miller, C. R. Mulvihill, B. Ruscic, Y. Tao, J. Zador and S. J. Klippenstein, *Theory Informed Kinetics (ThInK 1.0) Model for Core Combustion Species*, Spring Technical Meeting Eastern States Section of the Combustion Institute, 2024.
- 51 S. J. Klippenstein, *Proc. Combust. Inst.*, 2017, **36**, 77–121.
- 52 J. A. Miller, R. Sivaramakrishnan, Y. Tao, C. F. Goldsmith, M. P. Burke, A. W. Jasper, N. Hansen, N. J. Labbe, P. Glarborg and J. Zador, *Prog. Energy Combust. Sci.*, 2021, **83**, 100886.
- 53 A. Krisman, C. Mounaim-Rousellet, R. Sivaramakrishnan, J. A. Miller and J. H. Chen, *Proc. Combust. Inst.*, 2019, **37**, 1631–1638.
- 54 J. Zador, A. W. Jasper and J. A. Miller, *Phys. Chem. Chem. Phys.*, 2009, **11**, 11040–11053.
- 55 D. P. Zaleski, R. Sivaramakrishnan, H. R. Weller, N. A. Seifert, D. H. Bross, B. Ruscic, K. B. Moore, III, S. N. Elliott, A. V. Copan, L. B. Harding, S. J. Klippenstein, R. W. Field and K. Proszement, *J. Am. Chem. Soc.*, 2021, **143**, 3124–3142.
- 56 R. Sivaramakrishnan, J. V. Michael and S. J. Klippenstein, *J. Phys. Chem. A*, 2010, **114**, 755–764.

